Visualization of the birth of an optical vortex using diffraction from a triangular aperture

A. Mourka,[1] **J. Baumgartl,**[1] **C. Shanor,**[2] **K. Dholakia,**[1,2,*] **and E. M. Wright**[2,1]

[1]*SUPA, School of Physics and Astronomy, University of St. Andrews, North Haugh, St. Andrews KY16 9SS, UK*

[2] *College of Optics, University of Arizona, Tuscon, Arizona 85711, USA*

[*]*kd1@st-andrews.ac.uk*

Abstract: The study and application of optical vortices have gained significant prominence over the last two decades. An interesting challenge remains the determination of the azimuthal index (topological charge) ℓ of an optical vortex beam for a range of applications. We explore the diffraction of such beams from a triangular aperture and observe that the form of the resultant diffraction pattern is dependent upon both the magnitude and sign of the azimuthal index and this is valid for both monochromatic and broadband light fields. For the first time we demonstrate that this behavior is related not only to the azimuthal index but crucially the Gouy phase component of the incident beam. In particular, we explore the far field diffraction pattern for incident fields incident upon a triangular aperture possessing non-integer values of the azimuthal index ℓ. Such fields have a complex vortex structure. We are able to infer the birth of a vortex which occurs at half-integer values of ℓ and explore its evolution by observations of the diffraction pattern. These results demonstrate the extended versatility of a triangular aperture for the study of optical vortices.

OCIS codes: (050.1940) Diffraction; (140.3300) Laser beam shaping; (050.4865) Optical vortices; (050.1220) Apertures.

References and links

1. L. Allen, M. W. Beijersbergen, R. J. C. Spreeuw, and J. P. Woerdman, "Orbital angular momentum of light and the transformation of Laguerre–Gaussian laser modes," Phys. Rev. A **45**, 8185–8189 (1992).
2. J. F. Nye and M. V. Berry, "Dislocations in wave trains," Proc. R. Soc. Lond. A **336**, 165–190 (1974).
3. H. He, M. E. J. Friese, N. R. Heckenberg, and H. Rubinszstein-Dunlop, "Direct observation of transfer of angular momentum to absorptive particles from a laser beam with a phase singularity," Phys. Rev. Lett. **75**, 826–829 (1995).
4. K. Dholakia and W. M. Lee, "Optical trapping takes shape: the use of structured light fields," Adv. At. Mol. Phys. **56**, 261–337 (2008).
5. V. Garces-Chavez, D. McGloin, M. J. Padgett, W. Dultz, H. Schmitzer, and K. Dholakia, "Observation of the transfer of the local angular momentum density of a multiringed light beam to an optically trapped particle," Phys. Rev. Lett. **91**, 093602 (2003).
6. A. T. O'Neil, I. MacVicar, L. Allen, and M. J. Padgett, "Intrinsic and extrinsic nature of the orbital angular momentum of a light beam," Phys. Rev. Lett. **88**, 053601 (2002).
7. G. Molina-Terriza, J. P. Torres, and L. Torner, "Management of the angular momentum of light: preparation of photons in multidimensional vector states of angular momentum," Phys. Rev. Lett. **88**, 013601 (2001).

#140146 - $15.00 USD Received 23 Dec 2010; revised 14 Feb 2011; accepted 15 Feb 2011; published 14 Mar 2011

8. H. I. Sztul and R. R. Alfano, "Double-slit interference with Laguerre-Gaussian beams," Opt. Lett. **31**, 999–1001 (2006).
9. C. S. Guo, L. L. Lu, and H. T. Wang, "Characterizing topological charge of optical vortices by using an annular aperture," Opt. Lett. **34**, 3686–3688 (2009).
10. J. M. Hickmann, E. J. S. Fonseca, W. C. Soares, and S. Chavez-Cerda, "Unveiling a truncated optical lattice associated with a triangular aperture using lights orbital angular momentum," Phys. Rev. Lett. **105**, 053904 (2010).
11. S. S. R. Oemrawsingh, X. Ma, D. Voigt, A. Aiello, E. R. Eliel, G. W. 't Hooft, and J. P. Woerdman, "Demonstration of fractional orbital angular momentum entanglement of two photons," Phys. Rev. Lett. **95**, 240501 (2005).
12. I. V. Basistiy, M. Soskin, and M. V. Vasnetsov, "Optical wavefront dislocations and their properties," Opt. Commun. **119**, 604–612 (1995).
13. M. V. Berry, "Optical vortices evolving from helicoidal integer and fractional phase steps," J. Opt. A, Pure Appl. Opt. **6**, 259–268 (2004).
14. W. M. Lee, X. C. Yuan, and K. Dholakia, "Experimental observation of optical vortex evolution in a Gaussian beam with an embedded fractional phase step," Opt. Commun. **239**, 129–135 (2004).
15. J. Leach, E. Yao, and M. J. Padgett, "Observation of the vortex structure of a non-integer vortex beam," New J. Phys. **6**, 71 (2004).
16. R. C. Smith and J. S. Marsh, "Diffraction patterns of simple apertures," J. Opt. Soc. Am. **64**, 798–803 (1974).
17. A. E. Siegman, *Lasers* (University Science, 2004), Chap. 16.4.
18. J. Arlt, "Handedness and azimuthal energy flow of optical vortex beams," J. Mod. Opt. **50**, 1573–1580 (2003).

1. Introduction

In 1992 Allen *et al.* [1] recognized that certain optical fields may carry an angular momentum in addition to that associated with photon spin. Thus orbital angular momentum (OAM) was identified with Laguerre-Gaussian (LG) laser modes that possess an azimuthal phase. These are circularly symmetric transverse laser modes that form an orthonormal basis set and are characterized by two integer indices. The radial index is p with $p+1$ denoting the number of bright high intensity rings around the beam propagation axis. The azimuthal index ℓ characterizes the $\exp(\mathrm{i}\ell\varphi)$ phase dependence around the optical axis. It is sometimes denoted as the topological charge or winding number of the light field. The azimuthal index is commonly associated with the orbital angular momentum content of the beam given as $\ell\hbar$ per photon. More broadly, we may consider the field of optical vortices which relate to the presence of singular points in the optical field [2]. Such vortices appear in regions of darkness, i.e zero intensity. Thus whilst the high intense regions of the light field possess linear momentum or angular momentum, the vortices themselves do not have such attributes.

Such light fields have been the subject of intense study and potential ground-breaking applications over the last fifteen years. In particular they have found significant application in the fields of optical micromanipulation [3, 4, 5] where they may set microscopic particles into rotation, trapped low refractive index particles and created micropumps. These experiments have also elucidated the nature of the intrinsic and extrinsic nature of optical angular momentum [5, 6]. In the domain of quantum communication, LG modes have created much interest as they present a multi-dimensional Hilbert space and a spectrum of values of azimuthal index [7].

A key issue is the simple, direct measurement of the orbital angular momentum content of the light field. As an example this has been achieved using two slit interferometry. However issues may arise with the clarity of such a pattern and indeed how one might infer fractional ℓ values in such a system [8]. Circular apertures may be used but cannot distinguish between beams of opposite helicity but the same magnitude of azimuthal index [9].

In this paper we explore a method to measure the phase singularity of LG beams, based on the diffraction by a triangular aperture [10]. The results of this work reveal the orientation of the diffraction pattern in far-field from a triangular aperture illuminated by a LG beam which is a triangular lattice that depends crucially upon the sign and the magnitude of the azimuthal index ℓ which characterizes this beam. The azimuthal index ℓ can be determined in a simple and direct way from the form of the pattern. In particular, we demonstrate that the Gouy phase

#140146 - $15.00 USD Received 23 Dec 2010; revised 14 Feb 2011; accepted 15 Feb 2011; published 14 Mar 2011

shift causes the 180° rotation of the diffraction pattern as observed by Hickmann *et al.* [10] when changing the sign of the azimuthal index.

Recently, there has been significant interest in fractional azimuthal index dislocations embedded within optical beams for studies of entanglement and quantum information processing [11]. To date, for the generation of an optical beam of half-integer fractional index, both spiral phase plate and off-axis holograms, dynamic and static, have been used. Basistiy *et al.* [12] made use of a computer generated hologram, based on a half-integer screw dislocation, to generate a monochromatic beam. Berry [13] discussed mathematically the evolution of waves with phase singularities of $2p\ell$, where ℓ may now be either integer or non-integer. For the case of the fractional phase step ($2p\ell$) being non-integer, a key theoretical prediction of Berry is the birth of a vortex within the beam as the fractional phase step reaches and passes a half-integer value. Thus to experimentally investigate such fractional topological charges we need to both generalize the range of fractional phase steps available as well as find a way of studying the evolution. Experimental studies have been performed using interference [14, 15], however observation of the diffraction pattern from our triangular aperture offers a very simple route for exploration of this topic and we can deduce the birth and evolution of a vortex within the light field incident upon the triangular aperture.

2. Theoretical background

2.1. Basic equations

In this section we give the theoretical background necessary for discussing our experimental results. Our basic model involves diffraction of an incident monochromatic optical vortex of wavelength λ and azimuthal index ℓ that is centered on a polygonal aperture located at $z = 0$, z being the propagation axis. Denoting the transverse coordinates on the aperture plane as $(x,y) = (\rho,\theta)$ in either Cartesian or cylindrical polar coordinates, we write the aperture transmission function as $t(x,y) = t(\rho,\theta)$. For our specific case $t(x,y)$ describes an equilateral triangular aperture which has unity transmission inside the aperture and zero outside the aperture, and over the spatial extent of the aperture the slowly varying electric field envelope of the incident optical vortex at $z = 0$ is written as

$$\begin{aligned} E^{(\ell)}(x,y,0) &= A(x+\mathrm{i}\cdot\mathrm{sgn}(\ell)y)^{|\ell|} \\ &\equiv E^{(\ell)}(\rho,\theta,0) = A\rho^{|\ell|}e^{\mathrm{i}\ell\theta} \end{aligned} \tag{1}$$

where A measures the field strength, and we hereafter set $A = 1$. In our experiment we create the far-field diffraction pattern using a standard $2f$ Fourier transforming optical system based on a lens of focal length f, and we denote the transverse Cartesian coordinates in the focal plane as (ξ,η). The diffracted field at the distance $z = 2f$ past the aperture is then proportional to the Fourier transform of the product of the optical vortex times the aperture transmission function yielding the result [16]

$$E^{(\ell)}(X,Y,z) \propto \int_{-\infty}^{\infty} dx \int_{-\infty}^{\infty} dy t(x,y)(x+\mathrm{i}\cdot\mathrm{sgn}(\ell)y)^{|\ell|}e^{-\mathrm{i}(Xx+Yy)}, \tag{2}$$

where $X = 2\pi\xi/\lambda f$ and $Y = 2\pi\eta/\lambda f$ are scaled transverse coordinates in the observation plane.

We have numerically solved Eq. (2) using the discrete Fourier transform algorithm for the case of a triangular aperture and for a variety of input azimuthal indices ℓ, both integer values and non-integer. We checked our numerical code against the known analytic solution for a uniformly illuminated triangular aperture [16]. In the following sections we shall present numerical simulations of the far-field intensity profile $|E(X,Y,z)|^2$ for a variety of conditions. We

#140146 - $15.00 USD Received 23 Dec 2010; revised 14 Feb 2011; accepted 15 Feb 2011; published 14 Mar 2011

note that our main interest here is in the morphology of these intensity profiles, as opposed to the detailed intensity values or the specific spatial sizes. This is relevant in view of the fact that, within the paraxial approximations employed, the intensity profiles generated by Eq. (2) do not depend on the specific triangular aperture size but only on the azimuthal index ℓ. This follows from the fact that the optical vortices in Eq. (1) do not display any particular length scale against which the aperture could be compared.

2.2. Integer azimuthal indices

In a recent paper, Hickmann *et. al*. [10] have explored the properties of diffraction of optical vortices of integer azimuthal indices by triangular apertures and their use for measuring the azimuthal index. Here we repeat some of their findings for completeness in presentation, in particular that the diffraction pattern is rotated by 180° upon reversing the azimuthal index, and we explore the origin of this rotation which has not been done before. In Fig. 1 we show numerical simulations of the far-field intensity profile for azimuthal indices $\ell = 2,3,4$ in the upper row, and $\ell = -2,-3,-4$ in the lower row, and one observes what Hickmann *et al.* [10] refer to as truncated optical lattices. We have used the red-black color palette in Figs. 1 and 2 for direct comparison with our experimental results for which our camera uses this palette. From these simulations one can verify the rule that the number of interference lobes on any one side of the diffraction pattern is equal to the modulus of the azimuthal index plus one $(|\ell|+1)$. We also note that there are $(|\ell|+1)$ parallel rows or lines of lobes making up a given truncated optical lattice. Furthermore, the effect of changing the sign of the azimuthal index $\ell \to -\ell$ is to rotate the orientation of the truncated optical lattice by 180°, as can be verified by inspecting the upper and lower rows in Fig. 1. Thus the number of lobes in the truncated optical lattice and its orientation can be used as a detector of the azimuthal index of an incident optical vortex.

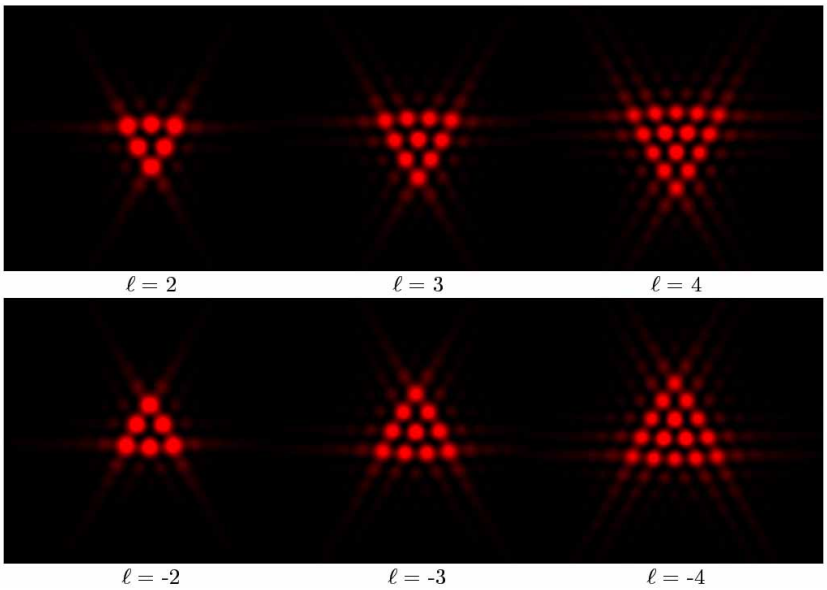

Fig. 1. Numerical simulations of the far-field intensity profile for azimuthal indices $\ell = 2,3,4$ in the upper row, and $\ell = -2,-3,-4$ in the lower row. These intensity patterns reveal the truncated optical lattice generated by the triangular aperture for incident optical vortices with integer azimuthal indices, and the fact that the intensity patterns are rotated by 180° under reversal of the sign of the azimuthal index.

#140146 - $15.00 USD Received 23 Dec 2010; revised 14 Feb 2011; accepted 15 Feb 2011; published 14 Mar 2011

It has previously been shown that a circular aperture can be used to detect the modulus of the azimuthal index of an optical vortex. The triangular aperture is even more flexible in that it can reveal both the magnitude and sign of the azimuthal index using the orientation of the intensity pattern [10]. This begs the question of the physical origin of the 180° rotation of the intensity pattern upon reversing the sign of the azimuthal index, and here we provide an answer to this question by demonstrating that the 180° rotation may be traced to the Gouy phase-shift. To begin with we consider a simpler free-space version of the model introduced in Sec. 2.1, both models yielding the Fourier transform of the field at the aperture. In the style of Eqs. (1) and (2) we here start with the electric field just beyond the aperture at $z = 0$

$$\begin{aligned} E^{(\ell)}(\rho,\theta,z=0) &= t(x,y)(x+\mathrm{i}\cdot\mathrm{sgn}(\ell)y)^{|\ell|} \\ &= t(\rho,\theta)\rho^{|\ell|}e^{\mathrm{i}\ell\theta}. \end{aligned} \tag{3}$$

In writing this we are explicitly assuming that the vortex core of the form $\rho^{|\ell|}e^{\mathrm{i}\ell\theta}$ is isolated by the aperture. To proceed we expand the field beyond the aperture in terms of the complete orthonormal set of LG modes

$$U_{p,m}(\rho,\theta,z) = u_{p,|m|}(\rho,z)e^{\mathrm{i}k\rho^2/2R(z)}e^{\mathrm{i}m\theta}e^{\mathrm{i}(2p+|m|+1)\Phi(z)}, \tag{4}$$

where the real functions $u_{p,|m|}(\rho,z)$ are given by [17]

$$u_{p,|m|}(\rho,z) = \left(\frac{2p!}{(1+\delta_{0,|m|})\pi(|m|+p)!}\right)\frac{1}{w(z)}\left(\frac{\sqrt{2}\rho}{w(z)}\right)^{|m|}L_p^{|m|}\left(\frac{2\rho^2}{w^2(z)}\right)e^{-\rho^2/w^2(z)}, \tag{5}$$

where $k = \omega/c$, $w(z)$ and $R(z)$ are the Gaussian spot size and radius of curvature of the propagating modes, $w(0) = w_0$ and $1/R(0) = 0$. $\Phi(z)$ is the Gouy phase-shift of the propagating modes, with $\Phi(0) = 0$ and $\Phi(z\to\infty) = \pi/2$. Then we may write the field beyond the aperture as an expansion of LG modes

$$E^{(\ell)}(\rho,\theta,z) = \sum_{p=0}^{\infty}\sum_{m=-\infty}^{\infty}C_{p,m}^{(\ell)}u_{p,|m|}(\rho,z)e^{\mathrm{i}k\rho^2/2R(z)}e^{\mathrm{i}m\theta}e^{\mathrm{i}(2p+|m|+1)\Phi(z)}, \tag{6}$$

where the expansion coefficients $C_{p,m}^{(\ell)}$ are evaluated at $z = 0$ and are given by

$$\begin{aligned} C_{p,m}^{(\ell)} &= \int_0^{\infty}\rho d\rho\int_0^{2\pi}d\theta E^{(\ell)}(\rho,\theta,0)U_{p,m}^{*}(\rho,\theta,0) \\ &= \int_0^{\infty}\rho d\rho\int_0^{2\pi}d\theta t(\rho,\theta)\rho^{|\ell|}e^{\mathrm{i}\theta(\ell-m)}u_{p,|m|}(\rho,0). \end{aligned} \tag{7}$$

We note that based on this definition the following symmetry holds that we shall use later

$$C_{p,m}^{(\ell)} = \left(C_{p,-m}^{(-\ell)}\right)^{*}, \tag{8}$$

and that this symmetry holds independent of the choice of LG spot size w_0. We now specifically consider the far-field for which the Gouy phase-shift is $\Phi(z)\to\pi/2$ [17], in which case the diffracted field becomes

$$\begin{aligned} E^{(\ell)}(\rho,\theta,z) &= e^{\mathrm{i}k\rho^2/2R(z)}\sum_{p=0}^{\infty}i(-1)^p\sum_{m=-\infty}^{\infty}C_{p,m}^{(\ell)}u_{p,|m|}(\rho,z)e^{\mathrm{i}(m\theta+|m|\pi/2)} \\ &= e^{\mathrm{i}k\rho^2/2R(z)}F^{(\ell)}(\rho,\theta,z), \end{aligned} \tag{9}$$

#140146 - $15.00 USD Received 23 Dec 2010; revised 14 Feb 2011; accepted 15 Feb 2011; published 14 Mar 2011

where

$$F^{(\ell)}(\rho,\theta,z)=\sum_{p=0}^{\infty} i(-1)^p \sum_{m=-\infty}^{\infty} C_{p,m}^{(\ell)} u_{p,|m|}(\rho,z) e^{\mathrm{i}(m\theta+|m|\pi/2)}. \tag{10}$$

The far-field intensity is therefore

$$I^{(\ell)}(\rho,\theta,z)=\left|E^{(\ell)}(\rho,\theta,z)\right|^2=\left|F^{(\ell)}(\rho,\theta,z)\right|^2. \tag{11}$$

Next we go through the same procedure for an incident field with azimuthal index $-\ell$ giving the far-field profile

$$\begin{aligned}
E^{(-\ell)}(\rho,\theta,z) &= e^{\mathrm{i}k\rho^2/2R(z)} \sum_{p=0}^{\infty} i(-1)^p \sum_{m=-\infty}^{\infty} C_{p,m}^{(-\ell)} u_{p,|m|}(\rho,z) e^{\mathrm{i}(m\theta+|m|\pi/2)} \\
&= e^{\mathrm{i}k\rho^2/2R(z)} \sum_{p=0}^{\infty} i(-1)^p \sum_{m=-\infty}^{\infty} C_{p,-m}^{(-\ell)} u_{p,|m|}(\rho,z) e^{\mathrm{i}(-m\theta+|m|\pi/2)} \\
&= e^{\mathrm{i}k\rho^2/2R(z)} \sum_{p=0}^{\infty} i(-1)^p \sum_{m=-\infty}^{\infty} \left(C_{p,m}^{(\ell)}\right)^* u_{p,|m|}(\rho,z) e^{-\mathrm{i}(m\theta+|m|\pi/2)} e^{\mathrm{i}m\pi} \\
&= e^{\mathrm{i}k\rho^2/2R(z)} \sum_{p=0}^{\infty} i(-1)^p \sum_{m=-\infty}^{\infty} \left(C_{p,m}^{(\ell)}\right)^* u_{p,|m|}(\rho,z) e^{-\mathrm{i}(m(\theta-\pi)+|m|\pi/2)} \\
&= e^{\mathrm{i}k\rho^2/2R(z)} \left[F^{(m)}(\rho,\theta-\pi,z)\right]^*,
\end{aligned} \tag{12}$$

where in the second line we switched $m\to -m$, in the third line we used the symmetry (8), and in the fourth line we used $e^{\mathrm{i}|m|\pi}=e^{\mathrm{i}m\pi}$. By comparing with Eq. (11), we therefore see that the far-field intensity pattern is given by

$$I^{(-\ell)}(\rho,\theta,z)=\left|F^{(\ell)}(\rho,\theta-\pi,z)\right|^2=I^{(\ell)}(\rho,\theta-\pi,z). \tag{13}$$

Thus the far-field intensity patterns for $\ell=\pm|\ell|$ have the structure given by $\left|F^{(\ell)}(\rho,\theta,z)\right|^2$ but are rotated by 180° with respect to each other around the vortex center. We note that if we artificially set the Gouy phase-shift to zero $\Phi(z)=0$ in the far-field in place of the correct value $\Phi(z)=\pi/2$, then the intensity pattern would not be rotated upon reversing the sign of ℓ, meaning that the rotation has its origin in the Gouy phase-shift. This is the main result of this analysis, and it explains the fact that diffraction of a optical vortex core from a polygonal aperture in general depends upon the sign of the azimuthal index, and furthermore exposes that this dependence stems from the Gouy phase-shift, giving new physical insight into this problem, compared to previous studies [10]. In conclusion the intensity pattern produced by a circular aperture is also rotated but this is clearly not observable, and the triangular aperture is likely the simplest aperture that can act as a detector of the magnitude and sign of the azimuthal index. We finally remark that Arlt [18] previously considered diffraction of an optical vortex by a knife edge as a detector of the absolute handedness of optical vortex beams.

2.3. Fractional azimuthal indices

We next turn to the second novel topic of this paper, namely the far field diffraction patterns obtained for incident fields possessing non-integer or fractional incident azimuthal indices ℓ. Figure 2 shows the intensity patterns obtained for $\ell=2\to 3$ in steps of 0.1. The main feature we wish to point out is that for azimuthal indices in the range $2<\ell<2.3$ the intensity pattern

#140146 - $15.00 USD Received 23 Dec 2010; revised 14 Feb 2011; accepted 15 Feb 2011; published 14 Mar 2011

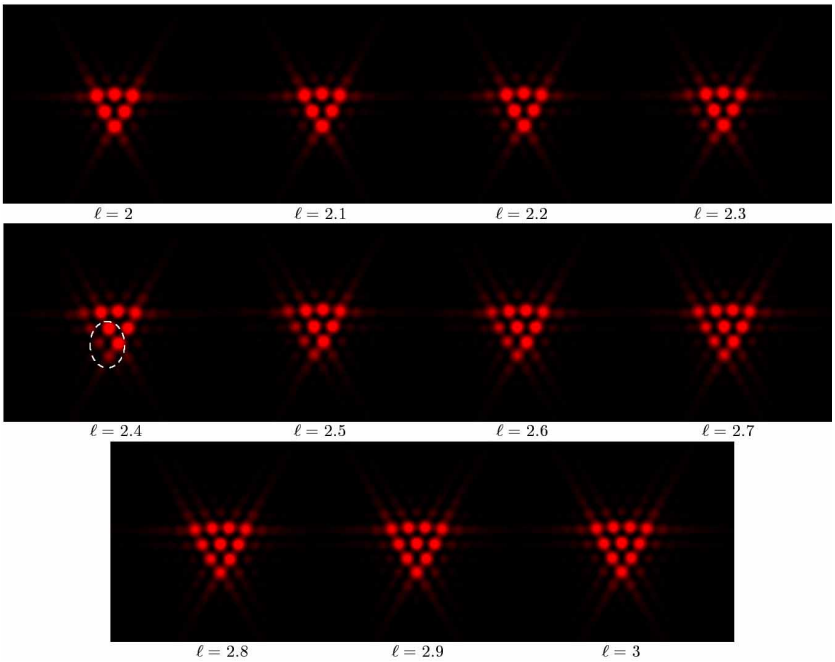

Fig. 2. Intensity patterns obtained for $\ell = 2 \rightarrow 3$ in steps of $\ell = 0.1$. These intensity patterns illustrate the birth of an optical vortex (region indicated by dashed ellipse) as the azimuthal index passes through a half-integer value.

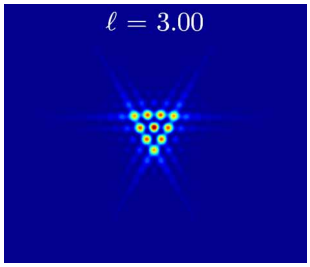

Fig. 3. (Media 1) The video includes an animation in which the intensity pattern is shown as the azimuthal index is varied from $\ell = 2 \rightarrow 5$, so that several examples can be viewed. To aid viewing the animation pauses at integer values of ℓ so that the reader can view the different examples involving variation between integer values of azimuthal index.

remains largely unchanged and close to that for $\ell = 2$ in that it has $(|\ell| + 1) = 3$ rows in the truncated optical lattice. In contrast for $\ell \geq 2.4$ one can see that the intensity pattern starts to distort on the left side as indicated by the circled region in the intensity pattern for $\ell = 2.4$ in Fig. 2. This distortion is the beginning of a new row of lobes that develops for $\ell > 2.4$, and for $\ell = 3$ the new row is fully formed and there are $(|\ell| + 1) = 4$ rows in the truncated optical lattice shown in the intensity profile. What the sequence of intensity profiles in Fig. 2 reveals is how the birth of a vortex is manifested in the truncated optical lattice generated by the triangular aperture, and in particular how the optical lattice deforms from having three to four rows as $\ell = 2 \rightarrow 3$ in this example: There is little distortion of the truncated optical lattice from its $\ell = 2$ form with 3 rows for $2 < \ell < 2.3$, and the birth of the $\ell = 3$ vortex with its 4 rows is

#140146 - $15.00 USD Received 23 Dec 2010; revised 14 Feb 2011; accepted 15 Feb 2011; published 14 Mar 2011

clearly evident for $\ell \geq 2.5$ until it is completed for $\ell = 3$. This sequence of events is perfectly in keeping with the prediction due to Berry [13] that the birth of a vortex occurs at the point where the fractional azimuthal index passes a half-integer value.

The above numerical results are easily generalized to higher azimuthal indices ℓ with the same general result: As the azimuthal index of the incident optical vortex passes $(|\ell| + 1/2)$ the birth of an optical vortex is revealed in the optical lattice produced by diffraction of the optical vortex by the triangular lattice, in keeping with Berry's prediction [13]. To illustrate this Fig. 3 provides an animation in which the intensity pattern is shown as the azimuthal index is varied from $\ell = 2 \rightarrow 5$, so that several examples can be viewed. To aid viewing the animation pauses at integer values of ℓ so that the reader can view the different examples involving variation between integer values of azimuthal index. The animation paints a fascinating picture in which starting from an integer ℓ azimuthal index the optical lattice has $(|\ell| + 1)$ rows which persist until the azimuthal index reaches $(|\ell| + 0.3)$ at which point the optical lattice appears to move to the right as a new row of lobes starts to appear on the left. This process culminates when the azimuthal index reaches $(|\ell| + 1)$ for which the optical lattice has $(|\ell| + 2)$ rows, and this scenario is seen in each example displayed in the animation.

The above simulations demonstrate that the optical lattice revealed in the intensity profiles generated from diffraction of an optical vortex by a triangular aperture can provide a visualization of the birth and evolution of an optical vortex as the azimuthal index is varied, and we next turn to the experimental realization of these results.

3. Experiments

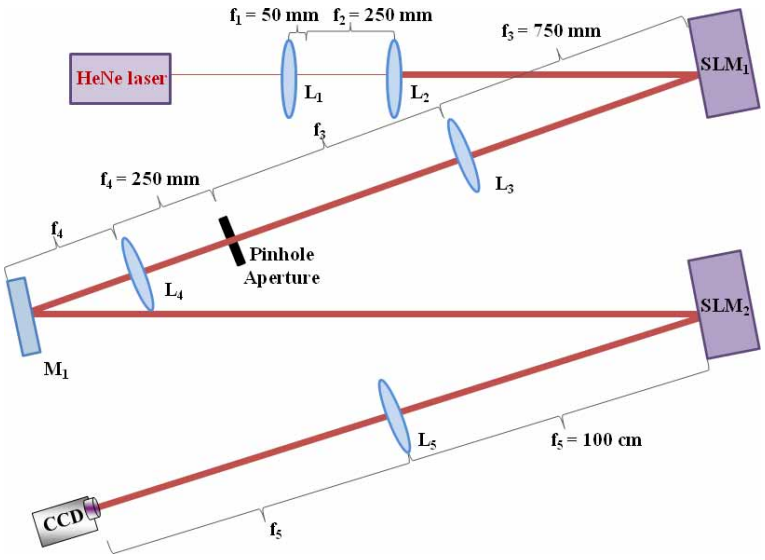

Fig. 4. Experimental setup for monochromatic studies: L = lens, SLM = spatial light modulator, M = mirror, CCD = Charge Coupled Device camera. Focal widths of lenses: $f_1 = 50$ mm, $f_2 = 250$ mm, $f_3 = 750$ mm, $f_4 = 250$ mm, $f_5 = 100$ cm. For the broadband studies, a prism in the back focal plane of L_4 compensated for dispersion mediated by the first SLM, and a static triangular aperture was used instead of the second SLM to avoid issues related to dispersion.

We have used the experimental setup shown in Fig. 4. A Helium Neon laser source (JDS Uniphase, 633 nm, $P_{\max} = 4$ mW) served for the monochromatic measurements and a supercon-

#140146 - $15.00 USD Received 23 Dec 2010; revised 14 Feb 2011; accepted 15 Feb 2011; published 14 Mar 2011

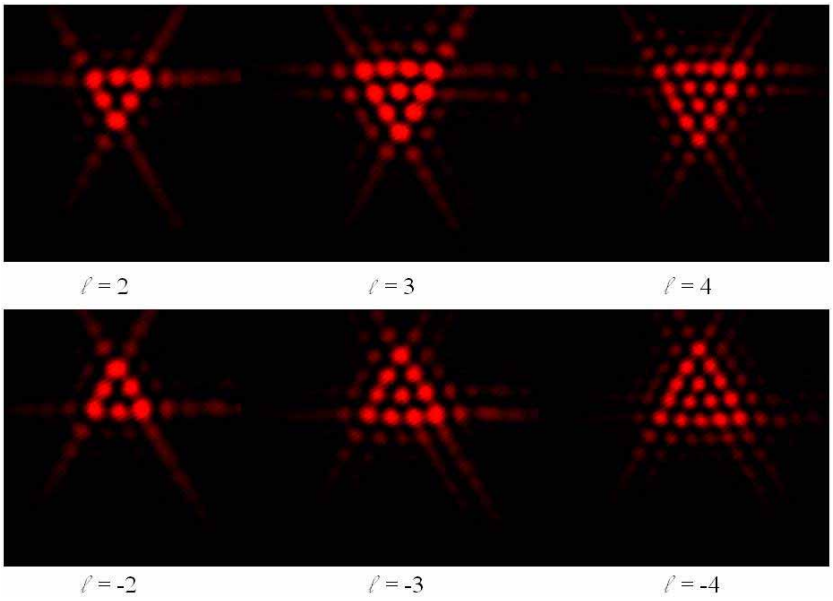

Fig. 5. Measured monochromatic far-field intensity profile for azimuthal indices $\ell = 2, 3, 4$ in the upper row, and $\ell = -2, -3, -4$ in the lower row. This should be compared to the theoretical prediction seen in Fig. 1.

tinuum source (Fianium Ltd, 4 ps, 10 Mhz) for the broadband white light measurements. The white light beam was additionally sent through a photonic crystal fiber (Thorlabs LMA-25) in order to obtain a beam featuring a homogeneous Gaussian intensity profile. The laser beam was subsequently expanded with a telescope in order to slightly overfill the chip of a spatial light modulator (SLM) which was a Holoeye LC-R 2500. The SLM operated in the standard first-order configuration and was used to imprint the vortex phase on the incident beam where the LG beam was created in the far-field of the SLM. We used a pair of lenses (lenses L_3 and L_4 in Fig. 4) in order to filter the first order beam, carrying the vortex, from the unmodulated zero-order beam using an aperture located in the back focal plane of lens L_3. For the broadband studies a prism (not shown in Fig. 4) was located in the back focal plane of lens L_4. With this, we compensated for the dispersion mediated by the linear phase shift imposed onto the laser beam by the SLM in order to separate the first-order from the zero-order beam. The two lenses are not necessary for the monochromatic studies, but we intended to perform both the monochromatic and the broadband studies on the basis of the same experimental setup. After lens L_4, the created LG beam was incident onto a triangular aperture located at a distance of approximately 3 m from lens L_4. The triangular aperture was realized in a different manner for the monochromatic and broadband studies. We used a second SLM (Hamamatsu X10468-01) for the monochromatic studies. This allowed us to flexibly change the geometry of the triangular aperture using dedicated Labview software. In particular, we were able to take into account the change in size of the LG beam when changing the index ℓ. In contrast, we used static triangular apertures imprinted onto photographic film for the broadband measurements. With this we avoided inducing dispersion onto the broadband LG beam which would require further prism compensation. Finally, lens L_5 was used to create the far-field diffraction pattern in the respective back focal plane where a color CCD camera (Basler piA640-210gc, pixel size: 7.4 μm $\times$ 7.4 μm) served to record and save images of the diffraction patterns onto the hard drive of a computer. On a final note, the quality of the prism dispersion compensation critically

#140146 - $15.00 USD Received 23 Dec 2010; revised 14 Feb 2011; accepted 15 Feb 2011; published 14 Mar 2011

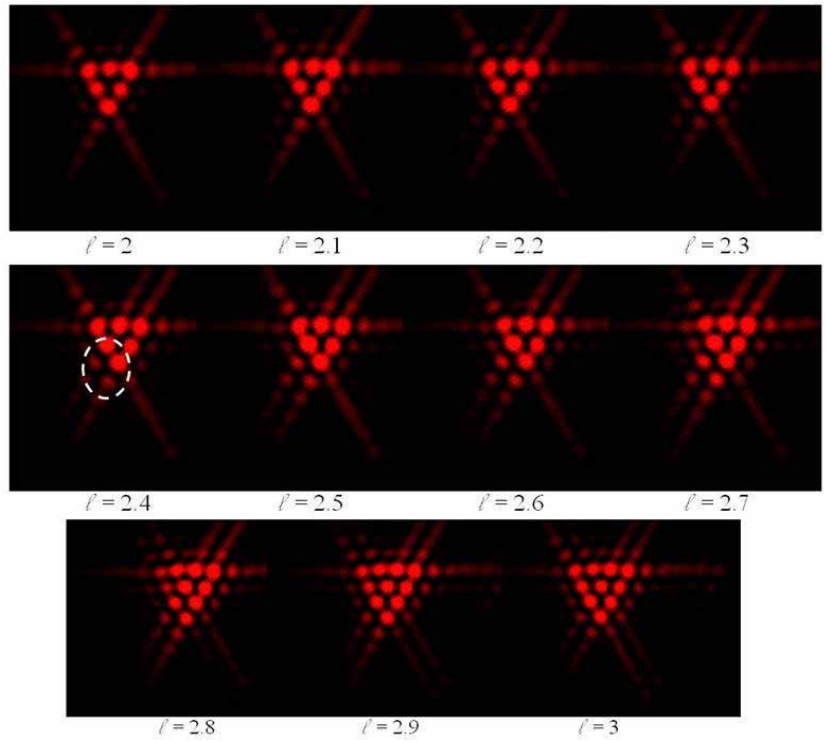

Fig. 6. Measured monochromatic far-field intensity patterns obtained for incident light fields with $\ell = 2 \rightarrow 3$ in steps of 0.1. The dashed ellipse indicates the region where the birth of the vortex is observed. Compare to theoretical prediction in Fig. 2.

depends on the beam diameter. To account for this, we reduced the size of the broadband LG beam by extracting a central part of the beam using the first SLM. We obtained satisfactory results in terms of dispersion compensation when reducing the beam diameter by a factor of 2.

To record distinct images of the monochromatic far-field diffraction patterns, we had to adjust both the size and thickness of the triangular aperture to the size of the LG beam under consideration since the diameter of the bright ring depends on the azimuthal index ℓ. The diffraction pattern is blurred and deformed if the size of the triangular aperture is not commensurate with the diameter of the bright ring. Moreover, the pattern intensity is larger for a large thickness while the pattern gets more distinct for a small thickness. We have also adjusted the CCD camera exposure time in order to best highlight the pattern morphology for each recorded pattern. We first show the experimental results for integer azimuthal indices in Fig. 5 where the triangular aperture was the same for $\ell = 2$ and $\ell = 3$ and adjusted to a larger size for $\ell = 4$. The experimental results are in excellent agreement with the theoretical prediction shown in Fig. 1: the number of interference lobes on any one side of the diffraction pattern is equal to $(|\ell| + 1)$, there are $(|\ell| + 1)$ parallel lines of lobes in any of the three directions, and the pattern orientation is flipped when the sign of the azimuthal index is changed. We also observe excellent agreement for non-integer azimuthal indices which is best seen through comparison of Figs. 6 and 2 where the former shows diffraction patterns recorded with the CCD camera for $\ell = 2 \rightarrow 3$ in steps of 0.1. The experimental data clearly manifest the expected distortion of the diffraction pattern for $\ell \geq 2.4$ as indicated by the circled region. A new row of lobes arises that develops for $\ell > 2.4$, and finally the $\ell = 3$ diffraction pattern is formed. Our experimental data there-

#140146 - $15.00 USD Received 23 Dec 2010; revised 14 Feb 2011; accepted 15 Feb 2011; published 14 Mar 2011

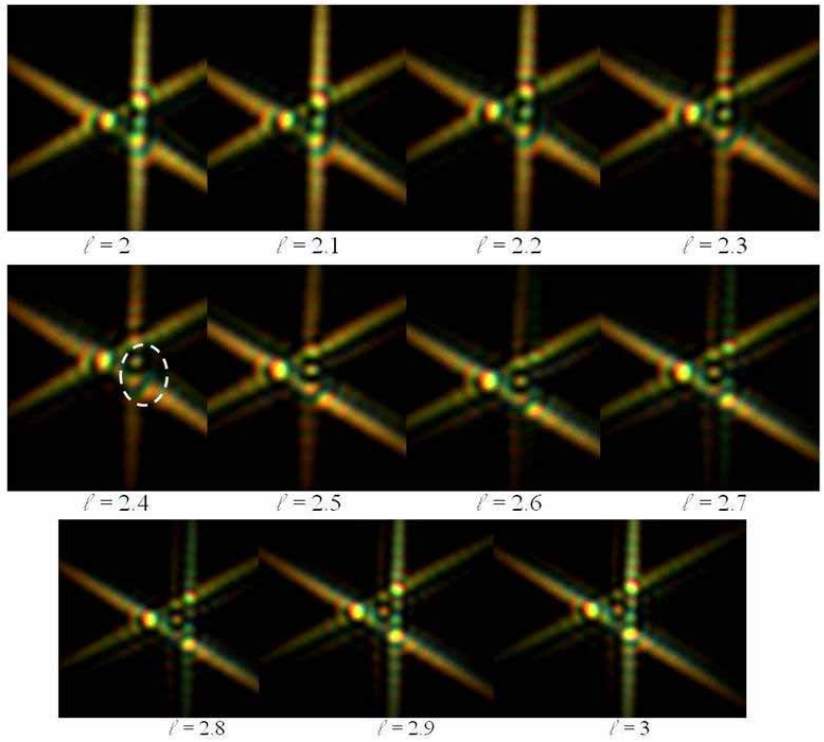

Fig. 7. Measured broadband intensity patterns obtained for $\ell = 2 \rightarrow 3$ in steps of 0.1. The dashed ellipse indicates the region where the birth of the vortex is observed. The discrepancy between the broadband and monochromatic data in terms of pattern orientation and region of vortex birth is explained in the final paragraph of this section 3.

fore verify Berry's prediction [13] of the birth of a vortex occurring at half-integer values of the fractional azimuthal index. We have also investigated whether the characteristic far-field diffraction patterns may be observed for broadband "white light" sources which feature a relatively poor temporal coherence. We show the broadband diffraction patterns for $\ell = 2 \rightarrow 3$ in steps of 0.1 in Fig. 7. The patterns are less distinct compared to the monochromatic data shown in Figs. 5 and 6 which, apart from the broadband nature of the light, must be attributed to the reduced LG beam size (only half of SLM display used due to dispersion compensation) and the use of static triangular apertures imprinted onto photographic film which did not allow us to adjust the aperture to the LG beam as flexibly as we were able to do in the monochromatic studies. Nevertheless, we can clearly identify the birth of the vortex in the broadband patterns as well and observe all the characteristic effects that is a new row of lobes arises for $\ell > 2.4$ as well.

We finally address an interesting question raised by our simulations and experiments: What decides the side of the optical lattice that distorts and finally leads to the creation of the new row following the birth of an optical vortex? In particular, for the case of integer azimuthal indices, the generated optical lattice is found to depend only on the orientation of the triangular aperture, and does not depend on any rotation of the optical vortex around its axis, this amounting to a trivial homogeneous phase-shift of the field. This is, however, not the case for fractional azimuthal indices for which the phase of the optical vortex $\exp(\mathrm{i}\ell\varphi)$ exhibits a discontinuity at a definite azimuthal angle that can be physically identified, so that the relative orientation of

#140146 - $15.00 USD Received 23 Dec 2010; revised 14 Feb 2011; accepted 15 Feb 2011; published 14 Mar 2011

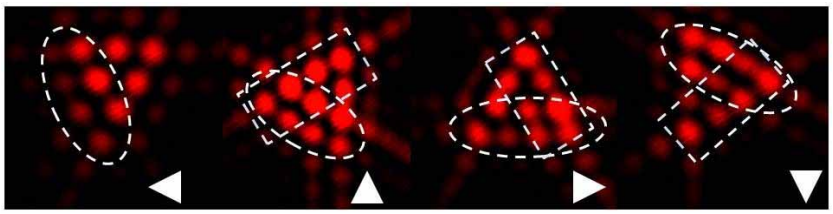

Fig. 8. Spatial dependency of the birth of the vortex on the orientation of the triangular aperture. The figure shows measured monochromatic intensity patterns obtained for $\ell = 2.6$ and different orientations of the triangular aperture as indicated on the right-bottom corner of the patterns. The dashed rectangles indicate where the birth of the vortex should be observed according to the rotation of the diffraction pattern. The dashed ellipse shows the spatial location where the birth of the vortex is actually observed.

the triangular aperture and azimuthal position comes into play and indeed dictates the spatial direction in which the optical lattice distorts and the lattice symmetry is broken. Thus, experimentally it should be the case that if the triangular aperture is rotated keeping the azimuthal index and orientation of the optical vortex fixed then the orientation of the optical lattice should also rotate. Moreover, the optical lattice should melt and reassemble at a different spatial location. This is indeed observed as we demonstrate in Fig. 8 on the basis of experimentally recorded monochromatic diffraction patterns. As the triangular aperture is rotated in steps of 90° so does the diffraction pattern. However, the region of the vortex birth does not follow the rotation as indicated by the dashed rectangles indicating the expected regions and the dashed ellipses indicating the actual regions where the birth of the vortex is observed. This observation also explains why the broadband data would not coincide with the monochromatic data if rotated accordingly. The monochromatic measurements were based on apertures created with a second SLM whereas the broadband measurements were performed using a static aperture. As a consequence, these two configurations exhibited different relative orientations between the aperture and the fractional vortex leading to different regions where the birth of the vortex took place.

4. Conclusions

We have explored the diffraction of light fields with various azimuthal indices from a triangular aperture. The behavior of the diffraction pattern is shown to be dependent upon the Gouy phase of the light field for the first time.The evolution and form of the far-field diffraction pattern from the triangular aperture for incident fields of fractional values of azimuthal index has also been explored. The experimental data show the methodology is applicable to both monochromatic and broadband light sources.

Acknowledgment

We thank the UK EPSRC for funding. KD is a Royal Society-Wolfson Merit Award Holder.

#140146 - $15.00 USD Received 23 Dec 2010; revised 14 Feb 2011; accepted 15 Feb 2011; published 14 Mar 2011